Theoretical & Applied Mechanics Letters 10 (2020) 125-131

Contents lists available at ScienceDirect

Theoretical & Applied Mechanics Letters

journal homepage: www.elsevier.com/locate/taml

Letter

Particle trajectories under interactions between solitary waves and a linear shear current

Xin Guan[a,b,*]

[a] *Key Laboratory for Mechanics in Fluid Solid Coupling Systems, Institute of Mechanics, Chinese Academy of Sciences, Beijing 100190, China*
[b] *School of Engineering Sciences, University of Chinese Academy of Sciences, Beijing 100049, China*

HIGHLIGHTS

- High-accuracy numerical solutions of full Euler equations are obtained.
- We used asymptotic expansions to obtain the classical Korteweg-de Vries equation, which provides a good quantitative description to the original problem when wave amplitude is small.
- We found two types of particle trajectories under solitary waves on a linear shear current, including periodic motions.

ARTICLE INFO

Article history:
Received 23 September 2019
Received in revised form 1 February 2020
Accepted 7 February 2020
This article belongs to the Fluid Mechanics.

Keywords:
Particle trajectories
Linear shear current
Solitary waves
Direct numerical simulation

ABSTRACT

This paper is concerned with particle trajectories beneath solitary waves when a linear shear current exists. The fluid is assumed to be incompressible and inviscid, lying on a flat bed. Classical asymptotic expansion is used to obtain a Korteweg-de Vries (KdV) equation, then a forth-order Runge-Kutta method is applied to get the approximate particle trajectories. On the other hand, our particular attention is paid to the direct numerical simulation (DNS) to the original Euler equations. A conformal map is used to solve the nonlinear boundary value problem. High-accuracy numerical solutions are then obtained through the fast Fourier transform (FFT) and compared with the asymptotic solutions, which shows a good agreement when wave amplitude is small. Further, it also yields that there are different types of particle trajectories. Most surprisingly, periodic motion of particles could exist under solitary waves, which is due to the wave-current interaction.

©2020 The Authors. Published by Elsevier Ltd on behalf of The Chinese Society of Theoretical and Applied Mechanics. This is an open access article under the CC BY-NC-ND license (http://creativecommons.org/licenses/by-nc-nd/4.0/).

Interactions between nonlinear water waves and currents play an important role not only in the mathematical theory of water waves, but also in our real life such as coastal and ocean engineering [1, 2]. In many cases of such phenomenon, for example, the motion of offshore platform in the ocean, it is necessary to study particle trajectories for some practical requirements, and this also helps us to better understand the flow structure beneath nonlinear waves.

When there is no current, it is well known that particles experience a backward-forward motion for periodic waves, following loops with a mean Stokes drift in the direction of wave propagation [3, 4]. On the other hand, all particles move in the direction of wave propagation without backward motion at all for solitary waves. This is proved by Constantin and Escher [5] based on a rigorous mathematical argument. Approximate analytical results were obtained by Borluk and Kalisch [6] and Gagnon [7] using the Korteweg-de Vries (KdV) equation. In the case of waves on currents with a uniform or sheared profile, mathematical properties of travelling waves have been established, including symmetry [8, 9], existence [10] and analyticity of streamlines [11]. The corresponding flow structure for small-amplitude periodic waves were also studied by Constantin and Villari [12], Ehrnström & Villari [13], and Wahlén [14]. Except for

* Corresponding author.
E-mail address: 13307130293@fudan.edu.cn (X. Guan).

http://dx.doi.org/10.1016/j.taml.2020.01.011
2095-0349/© 2020 The Authors. Published by Elsevier Ltd on behalf of The Chinese Society of Theoretical and Applied Mechanics. This is an open access article under the CC BY-NC-ND license (http://creativecommons.org/licenses/by-nc-nd/4.0/).

the Eulerian formulation, Zaman and Baddour [15], Chen et al. [16] and Hsu [17] used a Lagrangian formulation to describe wave-current interactions and particle trajectories. Their works yield that the mean level of a particle orbit over its period is higher than in the Eulerian formulation. Such inconsistency of two apparently equivalent systems has already been indicated by Provenzale et al. [18] in the study of particle trajectories under solitary waves, and they believed this difference comes from a mixing of perturbation order when using asymptotic expansions. On the other hand, periodic waves and solitary waves on a linear shear current has been widely studied based on the direct numerical simulation (DNS) (see [19–24] for example). Da Silva Teles et al. [19] used a boundary integral formulation to show that there exist closed streamlines or so-called cat's eyes in the frame of reference following waves. A similar result with respect to solitary waves with a shear current was also obtained by Johnson [25] using the asymptotic method. Same results were found analytically by Choi [26] using his strong nonlinear model, and by Ribeiro et al. [22] using a conformal map method. Kharif and Abid [27] proposed a new model derived from the Euler equations for fully nonlinear waves in the presence of linear shear current. From this model they derived a generalised Whitham equation which simplifies to the KdV equation previously obtained in Ref. [26]. At the same time, Hur [28] also derived shallow water wave models with constant vorticity and studied their stability. Curtis et al. [29] used a higher-order nonlinear schrödinger equation to study the effects of background shear on the modulational instability and particle trajectories. Most refereces cited above focused on the calculation of solitary waves, however, particle trajectories for solitary waves on a linear shear current through the direct numerical simulation (DNS) has rarely been studied so far, and this is what we focus on in this paper.

Consider an incompressible and inviscid fluid layer with constant density on a flat bed. The depth of the layer is h when the fluid is at rest. Inside the fluid there is a linear shear current so a constant vorticity with strength $-\omega$ exists everywhere. We set the undisturbed free surface to the level $z=0$, and the linear shear current is written as $U=\omega z$. We assume that a disturbance which has potential $\phi(t,x,z)$ occurs at some time and the free surface has an elevation $\eta(t,x)$, then we have the following governing equations:

In the domain $-h<z<\eta$:

$$\phi_{xx}+\phi_{zz}=0. \tag{1}$$

On the rigid bottom $z=-h$:

$$\phi_z=0. \tag{2}$$

On the free surface $z=\eta$:

$$\eta_t+\eta_x\Big(\phi_x+\omega\eta\Big)-\phi_z=0, \tag{3}$$

$$\phi_t+\frac{1}{2}\Big[\Big(\phi_x+\omega\eta\Big)^2+\phi_z^2\Big]+g\eta-\omega\Big(\psi+\frac{1}{2}\omega\eta^2\Big)=0, \tag{4}$$

where ψ is the complex conjugate of ϕ, and g is the gravitational acceleration. Our purpose is to solve η and ϕ, then calculate the particle trajectories.

Under the long-wave and small-amplitude assumption, we can derive the classical KdV equation. Assume the typical horizontal length scale is λ and introduce the typical velocity $c_0=\sqrt{gh}$, then the following Boussinesq scaling is chosen:

$$\begin{cases} x=\lambda x, \quad z=hz, \quad t=\dfrac{\lambda}{c_0}t, \quad \eta=a\eta, \\ \epsilon=\dfrac{a}{h}, \quad \mu=\dfrac{h}{\lambda}, \quad \phi=\epsilon c_0\lambda\phi, \quad \psi=c_0 a\psi. \end{cases} \tag{5}$$

The governing equations now become

$$\begin{cases} \mu^2\phi_{xx}+\phi_{zz}=0, & -1<z<\epsilon\eta, \\ \phi_z=0, & z=-1, \\ \eta_t+\epsilon\eta_x(\phi_x+\Omega\eta)-\dfrac{1}{\mu^2}\phi_z=0, & z=\epsilon\eta, \\ \phi_t+\dfrac{\epsilon}{2}\left(\phi_x^2+2\Omega\eta\phi_x+\dfrac{1}{\mu^2}\phi_z^2\right)+\eta \ -\Omega\psi=0,, & z=\epsilon\eta, \end{cases} \tag{6}$$

where $\Omega=\dfrac{\omega h}{c_0}$, $\epsilon\ll 1$, $\mu\ll 1$. In the subsequent calculation, the relation $\epsilon=\mu^2$ is chosen to balance nonlinearity and dispersion and the following asymptotic expansions of ϕ and ψ are assumed

$$\begin{cases} \phi=\displaystyle\sum_{n=0}^{\infty}(-1)^n\frac{\epsilon^n}{(2n)!}\frac{\partial^{2n}A}{\partial x^{2n}}(z+1)^{2n}, \\ \psi=\displaystyle\sum_{n=0}^{\infty}(-1)^n\frac{\epsilon^n}{(2n+1)!}\frac{\partial^{2n+1}A}{\partial x^{2n+1}}(z+1)^{2n+1}, \end{cases} \tag{7}$$

where $A=\phi(t,x,-1)$ represents the pontential function on the bottom. Substitute Eq. (7) into the two boundary conditions and we can obtain the following equation by neglecting the second-order terms

$$\begin{aligned} &A_{tt}-A_{xx}-\Omega A_{tx}-\epsilon\Big(\eta_x A_x+\Omega\eta\eta_x+\eta A_{xx}\Big) \\ &\quad-\epsilon\Big[\frac{1}{2}A_{ttxx}-\frac{1}{2}\Big(A_x^2\Big)_t-\frac{\Omega}{6}A_{txxx}-\frac{1}{6}A_{xxxx}\Big]=0. \end{aligned} \tag{8}$$

To obtain the KdV equation, the relation $\eta=-A_t+\Omega A_x+O(\epsilon)$ is used and Eq. (8) is rewritten by introducing new variables:

$$X=x-ct, \qquad T=\epsilon t, \tag{9}$$

where c by the linear terms in Eq. (8) satisfies

$$c^2+\Omega c-1=0. \tag{10}$$

Ultimately we have

$$A_{TX}+\frac{(\Omega^2+3)(c+\Omega)}{2c+\Omega}A_XA_{XX}+\frac{c^2}{3(2c+\Omega)}A_{XXXX}=0, \tag{11}$$

$$\eta_T+\frac{\Omega^2+3}{2c+\Omega}\eta\eta_X+\frac{c^2}{3(2c+\Omega)}\eta_{XXX}=0, \tag{12}$$

it is noted that Eq. (10) has been used to simplify the coefficients. Equation (12) is consistent with the equation obtained by Choi [26] after some variable transformation due to a different frame of reference. The travelling wave solutions are obtained immediately

$$\begin{cases} A_X = \gamma\delta^2 \mathrm{sech}^2(\delta(X-\upsilon T)), \\ \eta = (c+\Omega)\gamma\delta^2 \mathrm{sech}^2(\delta(X-\upsilon T)), \end{cases} \tag{13}$$

or equivalently

$$\begin{cases} A_x = \gamma\delta^2 \mathrm{sech}^2(\delta(x-(c+\epsilon\upsilon)t)), \\ \eta = (c+\Omega)\gamma\delta^2 \mathrm{sech}^2(\delta(x-(c+\epsilon\upsilon)t)), \end{cases} \tag{14}$$

where δ is a constant, $\gamma = \dfrac{4c^2}{(c+\Omega)(\Omega^2+3)}$ and $\upsilon = \dfrac{4\delta^2 c^2}{3(2c+\Omega)}$.

It is noted that the solitary waves are always of the elevation type, and for a fixed Ω there are two branches of solutions moving to right and left respectively.

To obtain particle trajectories, we need to solve the following nonlinear differential equations,

$$\begin{cases} u = \dfrac{\mathrm{d}x}{\mathrm{d}t} \approx \epsilon A_x + \Omega z, \\ w = \dfrac{\mathrm{d}z}{\mathrm{d}t} \approx -\epsilon A_{xx}(z+1), \end{cases} \tag{15}$$

and the forth-order Runge-Kutta method is used for the time integration. Here, to get some insights into the flow structure, it is convenient to choose a frame of reference moving with the wave, so we can approximate the stream function by

$$\Psi \approx \epsilon A_x(z+1) + \frac{\Omega}{2}z^2 - (c+\epsilon\upsilon)z. \tag{16}$$

It is interesting to note there exist closed streamlines. To see this, take the derivative of Eq. (16) with respect to z yields

$$\frac{\partial\Psi}{\partial z} \approx \epsilon A_x + \Omega z - c - \epsilon\upsilon. \tag{17}$$

On the vertical line $x = 0$, we have

$$\frac{\partial\Psi}{\partial z} \approx \epsilon\gamma\delta^2 + \Omega z - c - \epsilon\upsilon. \tag{18}$$

Note when Ω and c have different sighs, $\dfrac{\partial\Psi}{\partial z} = 0$ would has a root in the fluid domain, but this requires that ϵ is not too small since $|c/\Omega| > 1$. At $z \approx \dfrac{c+\epsilon\upsilon-\epsilon\gamma\delta^2}{\Omega}$, $w \approx 0$ and $u = 0$ due to the symmetry. So there exists a stagnation point and it is surrounded by a family of closed streamlines nearby.

To perform a DNS to the full Euler equations, a conformal map technique is used to map the physical domain onto a canonical strip, see also [22, 23]. The new variables ξ and ζ are introduced and the conformal map is defined as $F(\xi,\zeta) = x(\xi,\zeta) + \mathrm{i}z(\xi,\zeta)$. The free surface and the bottom are mapped to $\zeta = 0$ and $\zeta = -1$ respectively. For this purpose we need to solve the following boundary value problems

$$\begin{cases} z_{\xi\xi} + z_{\zeta\zeta} = 0, & -1 < \zeta < 0, \\ z = \eta(\xi), & \zeta = 0, \\ z = -1, & \zeta = -1, \end{cases} \tag{19}$$

and

$$\begin{cases} x_{\xi\xi} + x_{\zeta\zeta} = 0, & -1 < \zeta < 0, \\ x = X(\xi), & \zeta = 0, \\ x_\zeta = 0, & \zeta = -1. \end{cases} \tag{20}$$

These equations can be solved analytically. We take Eq. (19) for example. If we introduce $z' = z - \zeta$ which satisfies the corresponding homogeneous equation, and take the Fourier transform with respect to ξ, then we obtain an ordinary differential equation

$$\begin{cases} -k^2\hat{z}' + \hat{z}'_{\zeta\zeta} = 0, & -1 < \zeta < 0, \\ \hat{z}' = \hat{\eta}, & \zeta = 0, \\ \hat{z}' = 0, & \zeta = -1, \end{cases} \tag{21}$$

which has solution $\hat{z}' = \dfrac{\sinh(k(\zeta+1))}{\sinh(k)}\hat{\eta}$. By taking the inverse Fourier transform, we get the solution of Eq. (19)

$$z = \frac{1}{2\pi}\int_{-\infty}^{\infty} \frac{\sinh(k(\zeta+1))}{\sinh(k)}\hat{\eta}\mathrm{e}^{\mathrm{i}k\xi}\,\mathrm{d}k + \zeta, \tag{22}$$

similarly the solutioin of Eq. (20) is

$$x = \frac{1}{2\pi}\int_{-\infty}^{\infty} \frac{\cosh(k(\zeta+1))}{\cosh(k)}\hat{X}\mathrm{e}^{\mathrm{i}k\xi}\,\mathrm{d}k, \tag{23}$$

where the notation $\hat{z}'$, $\hat{\eta}$ and $\hat{X}$ denote the Fourier transform of z', η and X with respect to variable ξ in the sense of distribution (see Ref. [30, § 8]). Similarly, for ϕ and ψ we have

$$\begin{cases} \phi_{\xi\xi} + \phi_{\zeta\zeta} = 0, & -1 < \zeta < 0, \\ \phi = \Phi(\xi), & \zeta = 0, \\ \phi_\zeta = 0, & \zeta = -1, \end{cases} \tag{24}$$

and

$$\begin{cases} \psi_{\xi\xi} + \psi_{\zeta\zeta} = 0, & -1 < \zeta < 0, \\ \psi = \Psi(\xi), & \zeta = 0, \\ \psi = 0, & \zeta = -1, \end{cases} \tag{25}$$

the solutions are given by

$$\phi = \frac{1}{2\pi}\int_{-\infty}^{\infty} \frac{\cosh(k(\zeta+1))}{\cosh(k)}\hat{\Phi}\mathrm{e}^{\mathrm{i}k\xi}\,\mathrm{d}k, \tag{26}$$

$$\psi = \frac{1}{2\pi}\int_{-\infty}^{\infty} \frac{\sinh(k(\zeta+1))}{\sinh(k)}\hat{\Psi}\mathrm{e}^{\mathrm{i}k\xi}\,\mathrm{d}k. \tag{27}$$

According to the Cauchy-Riemann equation $x_\xi = z_\zeta$ and $\phi_\xi = \psi_\zeta$, we have the following identities on the free surface $\zeta = 0$

$$\widehat{X_\xi} = -\mathrm{i}\coth(k)\hat{\eta}_\xi + 2\pi\delta(k), \tag{28}$$

$$\widehat{\Phi_\xi} = -\mathrm{i}\coth(k)\widehat{\Psi_\xi}, \tag{29}$$

where $\delta(k)$ is the Dirac delta function. Since we are seeking travelling-wave solutions, it is convenient to choose a moving frame of reference so that waves become steady. Again we choose $\sqrt{gh}$ as the typical speed and other quantities are non-dimensionalised by

$$\begin{cases} x = hx, & z = hz, & t = \dfrac{h}{c_0}t, \\ \eta = h\eta, & \phi = c_0 h\phi, & \psi = c_0 h\psi. \end{cases} \tag{30}$$

Then the kinematic boundary condition and the Bernoulli

equation are

$$\eta_x(\phi_x+\Omega\eta-c)-\phi_z=0, \tag{31}$$

$$(\phi_x+\Omega\eta-c)^2+\phi_z^2+2\eta-c^2=0, \tag{32}$$

where Ω is defined as before. Using the new variables ξ and ζ, two boundary conditions can be recast to

$$\Psi+\frac{1}{2}\Omega\eta^2-c\eta=\text{const}, \tag{33}$$

$$\frac{\Phi_\xi^2+\Psi_\xi^2}{J}+\frac{2}{J}(\Phi_\xi X_\xi+\Psi_\xi\eta_\xi)(\Omega\eta-c)+2\eta +\Omega^2\eta^2-2c\Omega\eta=0, \tag{34}$$

where $J=x_\xi^2+z_\xi^2$. Equation (33) simply yields that the free surface is a streamline in the moving reference and it has been used to derive Eq. (32). So there is now only one independent equation, Eq. (34), in which X_ξ, Φ_ξ and Ψ_ξ are connected to η through Eqs. (28), (29) and (33).

To solve the nonlinear Eq. (34) numerically and obtain a travelling solitary wave solution, we take a long equally spaced grid points of ξ at $\zeta=0$:

$$\xi_n=-L+(n-1)\Delta\xi, \qquad n=1,2,\cdots,2N, \tag{35}$$

where $\Delta\xi=L/N$, and N is a large number. With an even symmetry of η about $\xi=0$, we actually have $N+1$ unknowns $\eta_i=\eta(\xi_i)$, $i=1,2,\cdots,N+1$. Together with the wave speed c under a given wave height H, this gives rise to a set of $N+1$ equations for $N+2$ unknowns $(\eta_1,\cdots,\eta_{N+1},c)$. The system is closed by adding the restriction about the wave height,

$$\eta_{N+1}-\eta_1=H. \tag{36}$$

Equations (34) and (36) are solved by Newton's method, with a small-amplitude solitary wave profile as initial guess. All the derivatives and integrals are calculated by their discrete Fourier representations using FFT. The Jacobian of the system for the Newton iteration is constructed by finite variations in the unknowns. The computation is stopped under the condition that the infinite norm of the system's deviation from zero is less than 10^{-10}.

There are two branches of solutions for a fixed value of Ω, corresponding to right-going waves and left-going waves. When Ω is replaced by $-\Omega$, the solutions are simply changed by reversing c to $-c$. So in our calculation, we always choose the branches with positive c.

When η and c are obtained, the whole velocity field can be calculated via Eqs. (22), (23), and (26)–(29). So the particle trajectories can be found by a time integral and we use the forth-order Runge-Kutta method.

To confirm the accuracy of DNS, we compare the values of wave speed c when different numbers of mesh points are considered in Table 1 firstly. For $\Omega=1(-10)$, $L=100(300)$ is chosen respectively. Excellent agreements are found, which shows the evidence of grid independence and high accuracy. Therefore, the results shown below are calculated with $N=2048$. In Fig. 1, we disply three branches of speed-amplitude bifurcation curves

Table 1 A quantitative comparsion of the numerical simulations with different numeber of spacial mesh points.

$\Omega=1$			$\Omega=-10$		
H	$c(N=1024)$	$c(N=2048)$	H	$c(N=1024)$	$c(N=2048)$
0.06	0.65184	0.65184	0.10	10.38856	10.38856
0.10	0.67377	0.67377	0.20	10.69546	10.69546
0.15	0.69963	0.69963	0.30	11.00048	11.00048
0.20	0.72271	0.72262	0.40	11.30254	11.30254
0.25	0.74247	0.73954	0.50	11.60154	11.60154

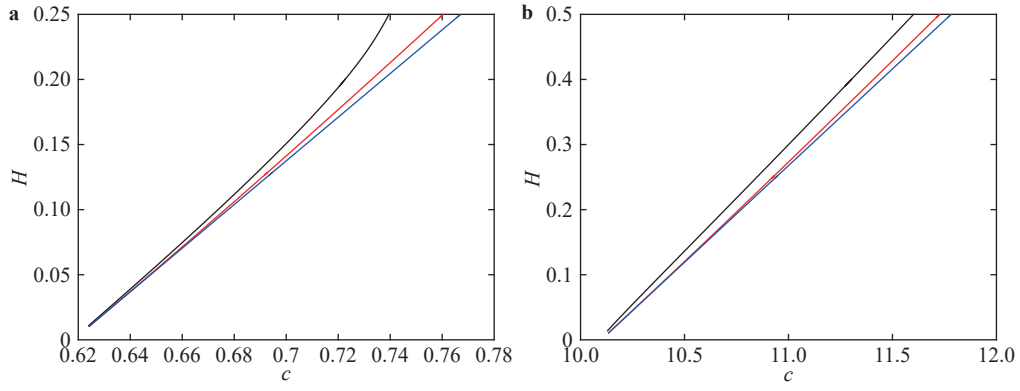

Fig. 1. A comparsion of three speed-amplitude bifurcation curves of solitary waves. Black: Euler model. Blue: KdV model. Red: Strong nonlinear model. In **a**: $\Omega=1$. In **b**: $\Omega=-10$.

which comes from Euler model, KdV model and Choi's strong nonlinear model [26]. As expected, the difference between them becomes considerable when H becomes large. But the great coincidence of weakly nonlinear case proves their validity.

In the following part we briefly display some of the results from the KdV model and DNS. In all the examples, we exhibit our results in two special frames of reference. One is the frame moving with solitary waves so that trajectories coincide with streamlines, the other is the still frame in which $\phi_x \to 0$ when $|x| \to \infty$.

When a constant vorticity exists, it is found that there are two types of streamlines in the moving frame of reference, which are open profile-shaped streamlines and closed streamlines respectively. The closed streamlines only exist under the condition that Ω and c have different signs. This coincides with our analysis of the stream function (16).

A typical result is shown in Fig. 2 with $\Omega = -10$ and different values of H. We compare the wave profiles and particle trajectories based on the KdV model and DNS respectively. In Fig. 2a, $H = 0.1$ and the KdV model provides a good quantitative description to the profiles and particle trajectories. The values of wave speeds are $c \approx 10.43$(KdV) and $c \approx 10.39$(DNS) respectively and the computing time periods of the particle trajectories are $[0,3]$, $[0,3]$ and $[0,23]$ from top to bottom. With H gradually increasing to 0.3, the difference between the model and DNS cannot be ignored in Fig. 2b. The wave speeds are $c \approx 11.1$(KdV) and $c \approx 11.0$ (DNS) with computing time periods are chosen $[0,3]$, $[0,3]$ and $[0,10.5]$ from top to bottom.

To see the different flow structure clearly, we choose two typical results and exhibit their streamlines in the moving frame of reference in Fig. 3. In Fig. 3a, $\Omega = 1$, $c \approx 0.73$. In this case, there are only open streamlines. In Fig. 3b, $\Omega = -10$, $c \approx 11.6$. When Ω and c have different signs, there could be a family of closed streamlines with a stagnation point inside. Calculation via Eq. (18) predicts the stagnation point is located at $z \approx 0.673$, which is quite close to the DNS result $z \approx 0.7$. Similar numerical result for periodic waves can be found in Refs. [19, 22]. This yields that there is a domain where particles are trapped, so they will move with the crest periodically. The corresponding particle trajectories in the still frame are shown in Fig. 4. In Fig. 4a, the linear shear current and solitary wave induce two flows in opposite directions. So the particles near the bottom are swept to the left by strong current. In Fig. 4b, the current near the bottom sweeps particles in front of solitary wave, where they have positive vertical velocity. After that they are exceeded by wave and then move downward, so periodic movements appear in this case.

In this paper, we focused on particle trajectories beneath solitary waves interacting with a linear shear current. Using the asymptotic expansion, we obtained the KdV equation and the travelling wave solutions of the velocity field. On the other hand,

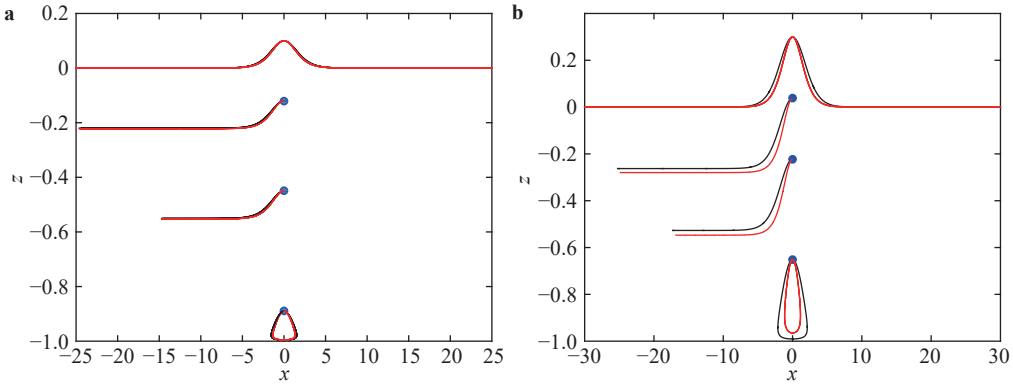

Fig. 2. Comparison of wave profiles and particle trajectories from the KdV model (red line) and DNS (black line). In both figures, $\Omega = -10$. The blue dots represent the start positions of the particles..

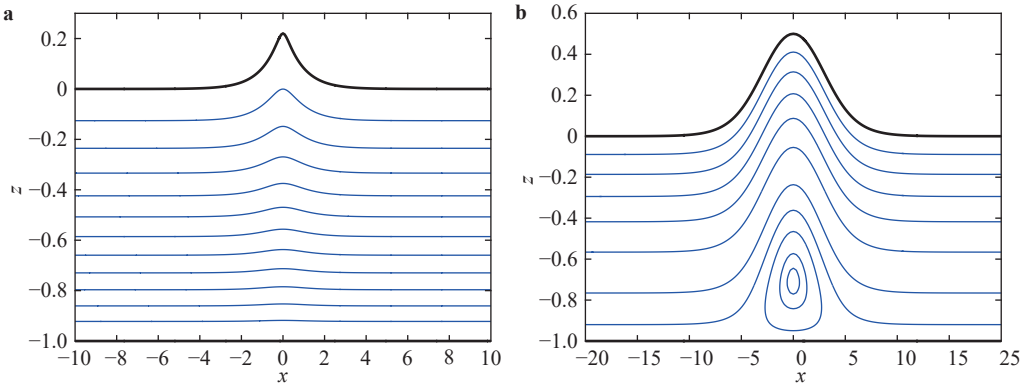

Fig. 3. Streamlines under the solitary waves in the moving frame. **a** $\Omega = 1$. **b** $\Omega = -10$. Different flow structures would appear depending on whether Ω and c have same or different signs.

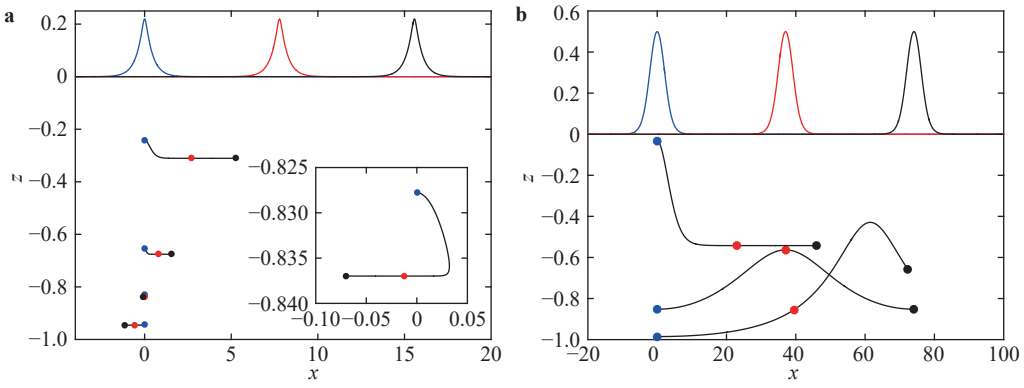

Fig. 4. Particle trajectories in the still frame. The blue dots and profiles represent the initial positions and profiles at $t = 0$, the red ones and black ones represent the positions and profiles at $t = t_{\mathrm{end}/2}$ and $t = t_{\mathrm{end}}$.

we performed a DNS to the original Euler equations via conformal map to obtain the high-accuracy numerical solutions. When wave amplitude is small, asymptotic solutions coincide well with numerical solutions. We also found that there are two types of particle trajectories. When Ω and c have same signs, the streamlines in the moving frame are quite similar to the case without current. When Ω and c are of opposite signs, closed streamlines can be found in the moving frame which yields periodic motions in the still frame.

Acknowledgement

This work was supported by the Key Research Program of Frontier Sciences, Chinese Academy of Sciences (No. QYZDBSS-WSYS015) and the Strategic Priority Research Program of the Chinese Academy of Sciences (No. XDB22040203). The author would also like to acknowledge the support from Chinese Academy of Sciences Center for Excellence in Complex System Mechanics.

References

[1] D.H. Peregrine, Interaction of water waves and currents, Adv. Appl. Mech. 16 (1976) 9–117.

[2] A. Constantin, E. Wărwărucă, Steady periodic water waves with constant vorticity: regularity and local bifurcation, Arch. Ration. Mech. Anal. 199 (2011) 33–67.

[3] G.G. Stokes, On the theory of oscillatory waves, Trans. Camb. Phil. Soc. 8 (1847) 533–583.

[4] A. Constantin, The trajectories of particles in stokes waves, Invent. Math. 166 (2006) 523–535.

[5] A. Constantin, J. Escher, Particle trajectories in solitary water waves, Bull. Amer. Math. Soc. 44 (2007) 42–431.

[6] H. Borluk, H. Kalisch, Particle dynamics in the kdv approximation, Wave Motion 49 (2012) 691–709.

[7] L. Gagnon, Qualitative description of the particle trajectories for the n-solitons solution of the korteweg-de vries equation, Discrete Contin. Dyn. Syst 37 (2017) 1489–1507.

[8] J.F. Toland, On the symmetry theory for stokes waves of finite and infinite depth, In Trends in Applications of Mathematics to Mechanics (Nice, 1998), Surv. Pure Appl. Math., 106 (2000) 207-217.

[9] A. Constantin, J. Escher, Symmetry of steady deep-water waves with vorticity, Eur. J. Appl. Math. 15 (2004) 755–768.

[10] A. Constantin, W. Strauss, E. Wărwărucă, et al, Global bifurcation of steady gravity water waves with critical layers, Acta Math. 217 (2016) 195–262.

[11] H. Lewy, A note on harmonic functions and a hydrodynamical application, Proc. Amer. Math. Soc. 3 (1952) 111–113.

[12] A. Constantin, G. Villari, Particle trajectories in linear water waves, J. Math. Fluid Mech. 10 (2008) 1–18.

[13] M. Ehrnström, G. Villari, Linear water waves with vorticity: rotational features and particle paths, J. Differ. Equ. 244 (2008) 1888–1909.

[14] E. Wahlén, Steady water waves with a critical layer, J. Differ. Equ. 246 (2009) 2468–2483.

[15] M.H. Zaman, E. Baddour, Interaction of waves with noncolinear currents, Ocean Eng. 38 (2011) 541–549.

[16] Y.Y. Chen, H.C. Hsu, H.H. Hwung, Particle trajectories beneath wave-current interaction in a two-dimensional field, Nonlinear Process Geophys. 19 (2012) 185–197.

[17] H.C. Hsu, Particle trajectories for waves on a linear shear current, Nonlinear Anal.-Real World Appl. 14 (2013) 2013–2021.

[18] A.Provenzale, A.R. Osborne, G. Boffetta, et al, Particle orbits from the lagrangian and the eulerian korteweg-de vries equations, Phys. Fluids 2 (1990) 866–869.

[19] A.F. Da Silva Teles, D.H. Peregrine, Steep, steady surface waves on water of finite depth with constant vorticity, J. Fluid Mech. 195 (1988) 281–302.

[20] J.-M. Vanden-Broeck, Steep solitary waves in water of finite depth with constant vorticity, J. Fluid Mech. 274 (1994) 339–348.

[21] W. Choi, Nonlinear surface waves interacting with a linear shear current, Math. Comput. Simul. 80 (2009) 29–36.

[22] R. Ribeiro, P.A. Milewski, A. Nachbin, Flow structure beneath rotational water waves with stagnation points, J. Fluid Mech. 812 (2017) 792–814.

[23] T. Gao, Z. Wang, P.A. Milewski, Nonlinear hydroelastic waves on a linear shear current at finite depth, J. Fluid Mech. 876 (2019) 55–86.

[24] T. Gao, P.A. Milewski, J.-M. Vanden-Broeck, Hydroelastic solitary waves with constant vorticity, Wave Motion 85 (2019) 84–97.

[25] R.S. Johnson, On the nonlinear critical layer below a nonlinear unsteady surface wave, J. Fluid Mech. 167 (1986) 327–351.

[26] W. Choi, Strongly nonlinear long gravity waves in uniform shear flows, Phys. Rev. E 68 (2003) 026305.

[27] C. Kharif, M. Abid, Nonlinear water waves in shallow water in the presence of constant vorticity: A whitham approach, Eur. J. Mech./B Fluids 72 (2018) 12–22.

[28] V. Hur, Shallow water models with constant vorticity, Eur. J. Mech./B Fluids 73 (2019) 170–179.

[29] C.W. Curtis, J.D. Carter, H. Kalisch, Particle paths in nonlinear schrödinger models in the presence of linear shear currents, J. Fluid Mech. 855 (2018) 322–350.

[30] W. Appel, Mathematics for Physics and Physicists, Princeton University Press, Princeton, NJ USA, 2007.